Adaptive Two-Degrees-of-Freedom Current Control for Solenoids: Theoretical Investigation and Practical Application

Michael Schwegel, Tobias Glück, *Member, IEEE*, Vitaly Shaferman, Luca Zaccarian, *Fellow, IEEE*, and Andreas Kugi, *Senior Member, IEEE*

***Abstract*— In this article, an adaptive two-degrees-of-freedom current control algorithm for solenoids is presented comprising an adaptive pole placement controller in combination with a regularized least-squares parameter estimation law. An additional adaptive feedforward controller takes advantage of the estimated plant parameters to further enhance the tracking performance. The stability of the overall closed-loop system is rigorously proven. The proposed solution differs from existing approaches by the adaptive feedforward controller and the way the parameter estimation is performed. The control concept is applied with the same controller parametrization to three solenoids from different applications, with substantially differing parameters. The experimental results show high tracking performance and fast parameter convergence even with poor initial estimates and despite the nonlinear dependence of the inductance on the current and position. The experimental results are also compared to two benchmark control design paradigms known from the literature, i.e. a second-order sliding mode controller and a nonlinear model reference adaptive control solution, which are both outperformed by the proposed controller.**

***Index Terms*— Adaptive control, least-squares identification, solenoid control, two-degrees-of-freedom control.**

I. Introduction

ADAPTIVE control can be used to mitigate control performance degradation due to manufacturing tolerances. In contrast to robust control, adaptive control aims at achieving high control performance even with varying, uncertain, or unknown system parameters. Moreover, adaptive control allows for the same controller to be employed within a class of structurally comparable systems. Due to the adaptive scheme, no manual adjustment of the controller parameters is necessary.

Parameter variations are common for solenoids, which are widely used in pneumatic and hydraulic drive systems for utility vehicles such as excavators and cranes as well as in vehicle powertrains and braking systems, see, e.g., [1], [2], [3], [4], [5]. In these applications, an adaptive controller can be employed to alleviate individual tuning procedures for different types of solenoid valves without compromising the tracking performance.

In the literature, different control approaches such as classical proportional integral (PI) or PI derivative (PID) control, internal model control (IMC), or sliding mode control (SMC) were investigated for the current control problem of solenoid valves. PID control and IMC are well-known standard control methods, which result in equivalent output control structures and are thus comparable in terms of their robustness and tracking performance. The main idea of SMC is the robust control of a system using a discontinuous feedback law, see, e.g., [6], [7], [8], [9]. This approach can robustly handle parameter variations, but typically requires a tailored tuning for a given system to meet the high demands on the closed-loop performance. High performance without individual tuning can be achieved by using adaptive control.

The adaptive output feedback control design problem for linear systems is well established and was solved in the late 90 s, see, e.g., the textbooks [10], [11], [12], [13]. Therein, three main approaches are distinguished: The first one is model reference adaptive control (MRAC) which is the adaptive version of the well-known model reference control (MRC) design. Here, the objective is to design a feedback controller that seeks to eliminate the output error between a reference model and the plant. The other two main approaches refer to direct and indirect adaptive control [10]. In direct adaptive control, the control parameters are adjusted directly to improve the control performance. Direct adaptive control approaches have the drawback that the parameters typically used for adaptation can hardly be interpreted from a physical point of view. In contrast, in indirect adaptive control, the plant parameters are estimated online and the control parameters are adjusted based on these estimates. These estimated plant

Manuscript received 14 December 2021; revised 3 August 2022; accepted 23 September 2022. Date of publication 18 October 2022; date of current version 25 April 2023. This work was supported in part by the Corporate Research of Robert Bosch GmbH. The authors acknowledge TU Wien Bibliothek for financial support through its open access funding program. *(Corresponding author: Michael Schwegel.)*

Michael Schwegel is with the Complex Dynamical Systems Group, TU Wien, 1040 Vienna, Austria (e-mail: michael.schwegel@tuwien.ac.at).

Tobias Glück is with the Center for Vision, Automation & Control, AIT Austrian Institute of Technology GmbH, 1210 Vienna, Austria (e-mail: tobias.glueck@ait.ac.at).

Vitaly Shaferman is with the Department of Aerospace Engineering, Technion - Israel Institute of Technology, Haifa 3200003, Israel (e-mail: vitalysh@technion.ac.il).

Luca Zaccarian is with the Department of Industrial Engineering, University of Trento, 38123 Trento, Italy, and also with the CNRS, Université de Toulouse, 31400 Toulouse, France (e-mail: zaccarian@laas.fr).

Andreas Kugi is with the Complex Dynamical Systems Group, TU Wien, 1040 Vienna, Austria, and also with the Center for Vision, Automation & Control, AIT Austrian Institute of Technology GmbH, 1210 Vienna, Austria (e-mail: kugi@acin.tuwien.ac.at).

Color versions of one or more figures in this article are available at https://doi.org/10.1109/TCST.2022.3211457.

Digital Object Identifier 10.1109/TCST.2022.3211457

parameters are not only instrumental for the parametrization of the controller but can also be employed for fault diagnosis and monitoring. New advances in hybrid and event-triggered adaptive control have targeted specific system classes such as systems with exogenous inputs in [14] or provided nonlinear methods which are numerically more expensive compared to classical control schemes, including the adaptive control strategy proposed in this article, see, e.g., [15].

The main purpose of adaptive control is to achieve high tracking performance despite unknown and/or changing system parameters. A well-known strategy to improve tracking performance is based on the idea of adding a feedforward path to an existing feedback control algorithm. Feedforward control is widely adopted, in particular in nonlinear adaptive control based on feedback linearization, see, e.g., [12], [16]. In these approaches, the parameter adaptation is mostly based on Lyapunov's theory, which guarantees convergence from a theoretical point of view but often results in an unsatisfactory slow convergence behavior in practical applications. Parameter adaptation based on least-squares methods ensures a balanced convergence rate across all parameters, see, e.g., [15]. These methods exhibit faster (second-order) convergence than typical Lyapunov-based approaches. Regularized recursive least-squares algorithms, see, e.g., [17], [18], mitigate the effect of noise on the parameter estimates by modifying the objective function and thus the gain matrix update to prevent the blow-up due to insufficient excitation [19], [20]. In recent works on robust least-squares system identification, non-asymptotic confidence intervals were computed [21], [22], [23], [24]. In addition, modifications of the least-squares algorithm known from the literature can be used to account for problem-specific challenges, such as structural uncertainties or unknown constraints, see, e.g., [18], [25], [26].

A. Contribution

This article aims at presenting a flexible and high-performance current control method for solenoids without position measurements at low computational costs. In particular, an indirect adaptive two-degrees-of-freedom control scheme for solenoids is presented. It consists of an adaptive feedforward and feedback path to fully take advantage of the estimated plant parameters. The plant parameters are estimated using a regularized least-squares adaptation law. Here, a reformulation and a modification of an adaptive control scheme are proposed to avoid the practical problems encountered when using the classical approach known from the literature, i.e. indirect adaptive control, see, e.g., [11], [12]. These modifications ultimately lead to a significant improvement in the control performance while maintaining the flexibility and ease of tuning of the original method.

The flexibility and the performance of the control scheme are experimentally demonstrated using three different solenoid types. Moreover, the proposed current control method is experimentally compared to other benchmark control methods known from the literature. It is shown that a robust second-order sliding mode controller requires retuning to achieve adequate control performance across multiple solenoid types. Furthermore, a nonlinear model reference adaptive control method serves as a benchmark for the assessment of the proposed control concept. It is demonstrated by the experimental results that this benchmark controller is outperformed by the proposed control scheme in both parameter convergence and control performance.

Summarizing, the main contribution of this article is threefold: First, an indirect adaptive control strategy known from the literature is reformulated to account for practical problems and enhance parameter convergence. Second, the adaptive control strategy is extended by an adaptive feedforward controller. The stability of the overall closed-loop system is proven. Third, an experimental validation underlining the practical value of the proposed control scheme is demonstrated by comparing the performance with two benchmark controllers from the literature.

B. Outline

The remainder of this article is organized as follows. In Section II, the problem is stated and the model of the solenoid current dynamics is presented. The adaptation framework and the necessary filtering are discussed in Section III-A, and the adaptive control law is given in Section III-B. The main stability theorems are summarized in Section IV. In Section V, two benchmark control approaches for the considered application are presented. Experimental validation and a comparison of the proposed control scheme with the benchmark controllers are presented in Section VI, followed by concluding remarks in Section VII. In Appendix A, the stability proof of the adaptive two-degrees-of-freedom controller is given and Appendix B contains the discrete-time implementation of the constrained bounded-gain forgetting least-squares algorithm, which is used for the parameter adaptation.

II. Problem Formulation

An adaptive current controller for solenoids is designed. A key concern is the achievable control performance without knowledge of the solenoid parameters. To reduce the costs, only the current i is measured, whereas the plunger position is not measured. Furthermore, since the nonlinear effects of a solenoid strongly depend on the respective design, these effects are not modeled.

Fig. 1 shows the simplified mechanical and electrical schematics of a solenoid. The setup comprises the moving plunger and the magnetic core with the associated coil. Both the plunger and the magnetic core are made of highly-permeable material with a relative permeability $\mu_r \gg 1$. The coil of the electromagnet is attached to the core and has N windings. Applying a voltage v to the terminals of the coil results in a current i, which in turn yields a magnetic field in the air gap g between the core and the position of the plunger. The coil voltage is typically provided by a high-side driver circuit. The generated pulsewidth modulated (PWM) voltage signal switches between the supply voltage

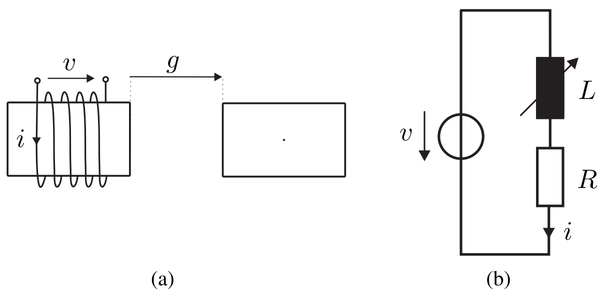

Fig. 1. Mechanical (a) and electrical (b) schematics of a solenoid.

v_{bat} and 0 V. Mathematically, the PWM voltage reads as

$$v(t) = \begin{cases} v_{\text{bat}} & \text{for, } \; kT_{\text{pwm}} < t \leq \big(k+\delta\big)T_{\text{pwm}} \\ 0\,\text{V} & \text{for, } \; \big(k+\delta\big)T_{\text{pwm}} < t \leq \big(k+1\big)T_{\text{pwm}} \end{cases} \tag{1}$$

for $k = 1, 2, 3, \ldots$ where $0 \leq \delta \leq 1$ is the duty cycle and T_{pwm} is the fixed modulation period.

For the magnetic flux linkage

$$\psi = L\big(g, i\big)i. \tag{2}$$

Faraday's law yields

$$\frac{\mathrm{d}\psi\big(g, i\big)}{\mathrm{d}t} = v - Ri \tag{3}$$

with the inductance $L(g, i)$ and the electrical terminal resistance R. Substituting (2) in (3) results in the current dynamics

$$\underbrace{\left(L\big(g, i\big) + \frac{\partial L\big(g, i\big)}{\partial i} i\right)}_{\bar{L}} \frac{\mathrm{d}i}{\mathrm{d}t} = v - \underbrace{\left(R + \frac{\partial L\big(g, i\big)}{\partial g}\dot{g}\right)}_{\bar{R}} i \; . \tag{4}$$

In practice, $\bar{L}$ and $\bar{R}$ are unknown nonlinear functions of the current i and the air gap g, which depend on the specific solenoid design. Recall that the objective of this article is to design an adaptive control strategy for (4) that exhibits the same closed-loop performance independent of $\bar{L}$ and $\bar{R}$. Since we do not have any information about the exact characteristics of $\bar{L}$ and $\bar{R}$, we assume for the controller design that $\bar{L}$ and $\bar{R}$ are unknown but constant. Note that this is a common assumption in the context of adaptive control in the literature, see, e.g., [27], [28] and the references therein. Thus, in the following, we focus on the simplified controller design model

$$\bar{L}\frac{\mathrm{d}y}{\mathrm{d}t} = u - \bar{R}y \tag{5}$$

with the average input voltage $u(t) = v_{\text{bat}}\delta(t)$, the unknown constant parameters $\bar{L}$ and $\bar{R}$, and the measured output current $y(t)$, which corresponds to the current $i(t)$ averaged over one modulation period.

Remark 1: It is worth noting that an adaptive controller that ensures stability and the desired closed-loop performance for (5) does not guarantee that this also holds true for (4). However, in this work an adaptive two-degrees-of-freedom control concept is presented where the feedforward part strongly predominates over the feedback part of the control input signal, see also the experimental results in Section VI-C.

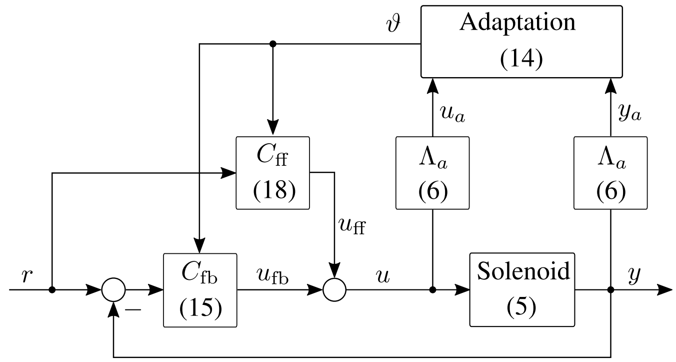

Fig. 2. Overall adaptive control structure with the filter Λ_a, the adaptive feedfoward controller C_{ff}, and the feedback controller C_{fb}.

This shows that the simplified model (5) together with the proposed parameter estimation approach is able to closely capture the dynamics of the original system (4). Note that it is well known from the literature, see, e.g., [29], [30], that parameter estimation schemes based on least-squares concepts with exponential forgetting exhibit certain robustness to unmodeled nonlinear dynamics and time-varying parameters.

III. Adaptive Control Concept

The proposed overall adaptive control structure is depicted in Fig. 2. The input u and the output y are filtered by the linear low-pass filter Λ_a to generate the signals for the parameter adaptation. The reference signal r, which is assumed to be two-times continuously differentiable, specifies the desired time evolution of the output current y. The estimated parameters $\boldsymbol{\vartheta}$ are fed back to parametrize the feedforward and feedback controller, denoted by C_{ff} and C_{fb}, respectively. Note, that we do not consider any disturbances affecting the plant in our setting, shown in Fig. 2.

A. Adaptation Scheme

To compute the time derivative of the current $y = x$ and to mitigate high-frequency measurement noise and unmodeled effects, (5) is filtered by the linear low-pass filter

$$\Lambda_a(s) = \frac{\lambda_a}{s + \lambda_a} \tag{6}$$

with the Laplace variable s and the filter constant $\lambda_a > 0$. The input-output behavior of the plant is preserved by filtering both signals

$$u_a = \Lambda_a u \quad \text{and} \quad y_a = \Lambda_a y \; . \tag{7a}$$

To apply a recursive least-squares algorithm, the model (5) is rewritten in the standard form with u_a as the scalar least-squares output, namely

$$u_a = \boldsymbol{\varphi}^{\mathrm{T}}\boldsymbol{\vartheta}^* = \begin{bmatrix} \frac{\mathrm{d}}{\mathrm{d}t}y_a & y_a \end{bmatrix} \begin{bmatrix} \bar{L} \\ \bar{R} \end{bmatrix} \tag{8}$$

where $\boldsymbol{\vartheta}^* \in \mathbb{R}^2$ is the true parameter vector and $\boldsymbol{\varphi} \in \mathbb{R}^2$ is the regression vector

$$\boldsymbol{\varphi} = \begin{bmatrix} \frac{\mathrm{d}}{\mathrm{d}t}y_a & y_a \end{bmatrix}^{\mathrm{T}}, \quad \boldsymbol{\vartheta}^* = \begin{bmatrix} \bar{L} & \bar{R} \end{bmatrix}^{\mathrm{T}} . \tag{9}$$

Remark 2: In the classical formulation of adaptation algorithms, the highest derivative of the system is chosen as the adaptation output, i.e. $\boldsymbol{\varphi}^{\mathrm{T}}\boldsymbol{\vartheta}^* = (\mathrm{d}/\mathrm{d}t)i_a$, see, e.g., [11], [12], which simplifies the mathematical treatment. In this case, the parameter vector reads as $\boldsymbol{\vartheta}^* = [1/\bar{L}, \bar{R}/\bar{L}]^{\mathrm{T}}$. Practical experiments showed that the resulting coupling between the inductance and resistance parameters drastically degrades the estimation performance. Compared to other formulations, in $\boldsymbol{\vartheta}^*$ of (9) the resistance and inductance can be estimated independently. In particular, since the resistance can be estimated in steady-state conditions, this formulation leads to a significant improvement in the robustness of parameter drifts caused by low excitation. Additionally, projection methods can be employed to guarantee strict bounds on the individual parameters.

Using the estimated parameter vector

$$\boldsymbol{\vartheta}^{\mathrm{T}} = \left[\hat{L}\ \hat{R}\right] \tag{10}$$

the estimation error ε can be introduced, based on (8) and (10), as

$$\varepsilon = \frac{\boldsymbol{\varphi}^{\mathrm{T}}\boldsymbol{\vartheta}^* - \boldsymbol{\varphi}^{\mathrm{T}}\boldsymbol{\vartheta}}{m^2} = \frac{u_a - \boldsymbol{\varphi}^{\mathrm{T}}\boldsymbol{\vartheta}}{m^2} \tag{11}$$

with the normalization factor $m^2 = 1 + \boldsymbol{\varphi}^{\mathrm{T}}\boldsymbol{\varphi}$, see, e.g., [11]. Note that the normalization can be omitted if $\boldsymbol{\varphi} \in \mathcal{L}_\infty$, i.e., the vector function $\boldsymbol{\varphi}$ is essentially bounded. However, using the normalization factor m the adaptation speed is normalized, which facilitates parameter tuning of the adaptation algorithm. In addition, to guarantee feasible limits of the parameter estimates, such as positive values for the inductance and resistance estimates, projection allows handling convex parameter constraints $\boldsymbol{\vartheta} \in \mathcal{S}$. Given a convex set $\mathcal{S}$, the orthogonal projection of $\boldsymbol{\vartheta}$ on the set $\mathcal{S}$ is the solution to the optimization problem

$$\mathcal{P}_{\boldsymbol{\vartheta}}\left(\boldsymbol{\vartheta}\right) = \arg\min_{\mathbf{v}\in\mathcal{S}} \|\mathbf{v} - \boldsymbol{\vartheta}\|_2^2 . \tag{12}$$

One can define the projection of a vector $\mathbf{z}$ by, see [31]

$$\Pi_{\boldsymbol{\vartheta}}\left(\boldsymbol{\vartheta}, \mathbf{z}\right) = \lim_{\eta\to 0} \frac{\mathcal{P}_{\boldsymbol{\vartheta}}\left(\boldsymbol{\vartheta} + \eta\mathbf{z}\right) - \boldsymbol{\vartheta}}{\eta} \tag{13}$$

with the convex set $\mathcal{S} = \{\boldsymbol{\vartheta} \in \mathbb{R}^2 | \mathbf{g}(\boldsymbol{\vartheta}) \leq \mathbf{0}\}$, its boundary $\delta\mathcal{S}$ and interior $\mathcal{S}^\circ$. Herein the inequality $\mathbf{g}(\boldsymbol{\vartheta}) \leq \mathbf{0}$ describes the set $\mathcal{S}$ in the parameter space. To estimate the parameter vector $\boldsymbol{\vartheta}$, the so-called continuous-time constrained bounded-gain forgetting least-squares algorithm from [17] is augmented with the projection algorithm described above. Following similar steps to those in [18], this yields

$$\frac{\mathrm{d}}{\mathrm{d}t}\boldsymbol{\vartheta} = \Pi_{\boldsymbol{\vartheta}}\left(\boldsymbol{\vartheta}, \mathbf{P}\boldsymbol{\varphi}\varepsilon\right), \quad \boldsymbol{\vartheta}(0) = \boldsymbol{\vartheta}_0 \tag{14a}$$

$$\frac{\mathrm{d}}{\mathrm{d}t}\mathbf{P} = \Pi_{\mathbf{P}}\left(\boldsymbol{\vartheta}, \beta\mathbf{P} - \mathbf{P}\frac{\boldsymbol{\varphi}\boldsymbol{\varphi}^{\mathrm{T}}}{m^2}\mathbf{P}\right), \quad \mathbf{P}(0) = P_0\mathbf{I} \tag{14b}$$

with

$$\Pi_{\mathbf{P}}\left(\boldsymbol{\vartheta}, \cdot\right) = \begin{cases} \cdot, & \text{if } \boldsymbol{\vartheta} \in \mathcal{S}^\circ \text{or}\left(\text{if } \boldsymbol{\vartheta} \in \delta\mathcal{S} \text{ and}\left(\mathbf{P}\boldsymbol{\varphi}\varepsilon\right)^{\mathrm{T}}\nabla\mathbf{g} \leq \mathbf{0}\right) \\ \mathbf{0}, & \text{otherwise} . \end{cases} \tag{14c}$$

Herein, $\mathbf{P}$ is the positive definite gain matrix, $\boldsymbol{\vartheta}_0$ and $P_0\mathbf{I} > 0$ are the initial conditions, and $\mathbf{I}$ denotes the identity matrix. The (time-dependent) forgetting factor

$$\beta = \beta_{\max}\left(1 - \frac{\|\mathbf{P}\|}{P_{\max}}\right) \tag{14d}$$

with $P_{\max}$ being an arbitrary positive constant, in (14b) guarantees an upper and lower bound on the gain matrix $\mathbf{P}$ and a maximum forgetting factor of $\beta_{\max}$, see [17]. For a more detailed analysis of least-squares adaptation algorithms, see, e.g., [18], [32], further a practical implementation is given in Appendix B. The upper bound on the norm of the gain matrix can be specified by $P_{\max} > 0$. The parameters $\beta_{\max}$, $P_{\max}$, and the filter constant λ_a in (6) allow for an independent tuning of the adaptation algorithm. Hence, strong filtering can be used to suppress noise and filter unmodeled system dynamics. Analogous to a conventional discrete-time least-squares forgetting factor $\lambda \in (0, 1]$, see, e.g., [33], the continuous-time forgetting factor can be found by $\beta_{\max} = (1 - \lambda)/T_s$, with the sampling time T_s, cf. (48e). The maximum gain $P_{\max}$ allows limiting the gradient of the estimated parameters.

B. Feedback and Feedforward Control

Using the certainty equivalence principle, adaptive pole placement control, see, e.g., [11], allows to derive the adaptive PI-feedback controller

$$u_{\mathrm{fb}} = \hat{k}_p e + \hat{k}_i x_c \tag{15a}$$

$$\dot{x}_c = e \tag{15b}$$

with the control error

$$e = r - y \tag{16}$$

and the known reference signal r. The adaptive feedback controller (15) constitutes a PI controller with time-varying proportional and integral gains parametrized by adaptive pole placement according to

$$\hat{k}_p = \hat{L}\alpha_1^* - \hat{R} \quad \text{and} \quad \hat{k}_i = \hat{L}\alpha_0^* \tag{17}$$

respectively, with constant coefficients $\alpha_1^* > 0$ and $\alpha_0^* > 0$. To enhance the tracking performance, the adaptive feedforward controller

$$u_{\mathrm{ff}} = \hat{L}\dot{r} + \hat{R}r \tag{18}$$

is introduced. Finally, the adaptive two-degrees-of-freedom control input is given by

$$u = u_{\mathrm{ff}} + u_{\mathrm{fb}} . \tag{19}$$

Applying (19), with (15)–(18), to (5) and assuming that the certainty equivalence holds, i.e. the estimated parameters $\hat{L}$ and $\hat{R}$ correspond to their real values $\bar{L}$ and $\bar{R}$, respectively, the closed-loop error system

$$\ddot{e} + \alpha_1^*\dot{e} + \alpha_0^* e = 0 \tag{20}$$

is obtained. Clearly, with the constants α_0^* and α_1^* the closed-loop poles of the error dynamics (20) can be chosen to achieve an exponentially stable behavior with a desired rate of decay.

Now the feedforward and feedback control (19) with (15)–(18) is combined with the parameter adaptation algorithm (14) to form the overall adaptive control scheme of Fig. 2.

IV. Stability Proof in a Nutshell

In this section, the main points of the stability proof of the overall closed-loop system comprising adaptation, controller, and plant are outlined. The only assumptions made are that the ideal parameter vector $\boldsymbol{\vartheta}^*$ is constant and that the reference signal r is sufficiently smooth, i.e., $r, \dot{r}, \ddot{r} \in \mathcal{L}_\infty$. Under these assumptions, we can state Theorem 1, which guarantees bounds on certain signals of the adaptation algorithm.

Theorem 1: The least-squares algorithm (14) guarantees that

1) $\varepsilon, \dot{\boldsymbol{\vartheta}}, \boldsymbol{\vartheta}, \varepsilon m, \mathbf{P} \in \mathcal{L}_\infty$
2) $\varepsilon, \dot{\boldsymbol{\vartheta}}, \varepsilon m \in \mathcal{L}_2$
3) $\mathbf{g}(\boldsymbol{\vartheta}) \leq \mathbf{0}$,

with $\mathcal{L}_2$ being the space of quadratically integrable functions and $\mathcal{L}_\infty$ the space of essentially bounded functions.

Proof: The proof of Theorem 1 is similar to what is shown in [11] and follows by analyzing the function $V = (\boldsymbol{\vartheta} - \boldsymbol{\vartheta}^*)^{\mathrm{T}}\mathbf{P}^{-1}(\boldsymbol{\vartheta} - \boldsymbol{\vartheta}^*)$. □

Finally, Theorem 2 establishes the asymptotic stability of the overall adaptive control scheme of Fig. 2.

Theorem 2: For the parameter estimation algorithm presented in (14), all signals in the closed-loop adaptive two-degrees-of-freedom control system (14)–(19) are uniformly bounded and the control error e converges asymptotically to zero.

Proof: The proof of Theorem 2 is performed in four steps.

1) First, the estimation error and control law are expressed as a linear time-varying (LTV) system.
2) Second, exponential stability of the LTV system is shown.
3) Third, the boundedness of all signals in the closed-loop system is established by using the Bellman-Gronwall lemma.
4) Finally, the control error convergence is proven using Barbalat's lemma.

More details of the proof are given in Appendix A. □

Remark 3: Assuming the persistence of excitation of the regression vector $\boldsymbol{\varphi}$, the adaptation algorithm converges exponentially to the ideal parameter vector, see [18]. However, for the convergence of the control error e neither persistence of excitation nor convergence of the parameters to the ideal parameter vector are necessary, as stated in Theorem 2.

V. Benchmark Approaches From the Literature

In the following sections, two benchmark control approaches from the literature are presented and their performance is compared with the adaptive two-degrees-of-freedom control algorithm presented in this article. First, in Section V-A, a second-order sliding mode controller is given as an example of a robust control method commonly employed in solenoid control. Second, a model reference adaptive controller serving as a benchmark for an adaptive control method is discussed in Section V-B. In industrial applications, further measures are taken to avoid practical problems like parameter drift under steady-state conditions, e.g. deadzone, dynamic normalization, or anti-windup, see, e.g., [11, chap. 8] for more details. In the following, for the sake of a fair and meaningful comparison, we refrain from implementing such measures because they can be used independently of the respective control method.

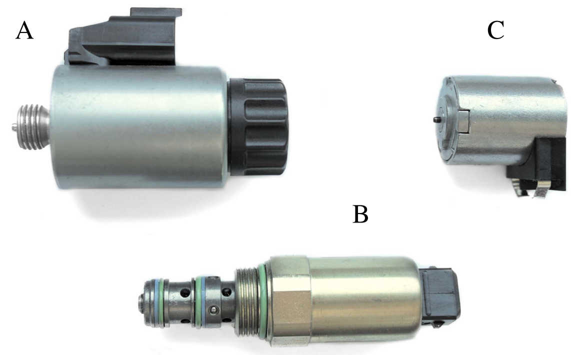

Fig. 3. Photographs of the solenoids used for the experimental validation.

TABLE I
Nominal Parameters of the Solenoids of Fig. 3

	Solenoid A	Solenoid B	Solenoid C
$\bar{R}$	R_A	$0.47R_A$	$0.82R_A$
$\bar{L}$	L_A	$0.15L_A$	$0.23L_A$

TABLE II
Parameters Used for the Sliding Mode Controller Experiments

Control		Sliding surface	
α_1	0.35	λ_1	20
α_0	0.04	λ_0	100

A. Second-Order Sliding Mode Controller

A second-order sliding mode controller with dynamic pole placement is proposed in [6]. The control input

$$u = \alpha_1\sqrt{|\sigma(t)|}\,\mathrm{sign}\big(\sigma(t)\big) + \alpha_0\int_0^t \sqrt[3]{|\sigma(\tau)|}\,\mathrm{sign}\big(\sigma(\tau)\big)\,\mathrm{d}\tau \tag{21a}$$

with the constant tuning parameters $\alpha_0 > 0$ and $\alpha_1 > 0$ and the control error $e(t) = r(t) - y(t)$ is used to stabilize the sliding surface

$$\sigma(e) = \left(\frac{\mathrm{d}}{\mathrm{d}t} + \lambda_0 - \lambda_1|e|\right)e \tag{21b}$$

with the constant tuning parameters $\lambda_1 > 0$ and $\lambda_0 > 0$. The bounds $|e| < e_{\max}$ and $\lambda_0 > \lambda_1 e_{\max}$ guarantee a stable closed-loop system.

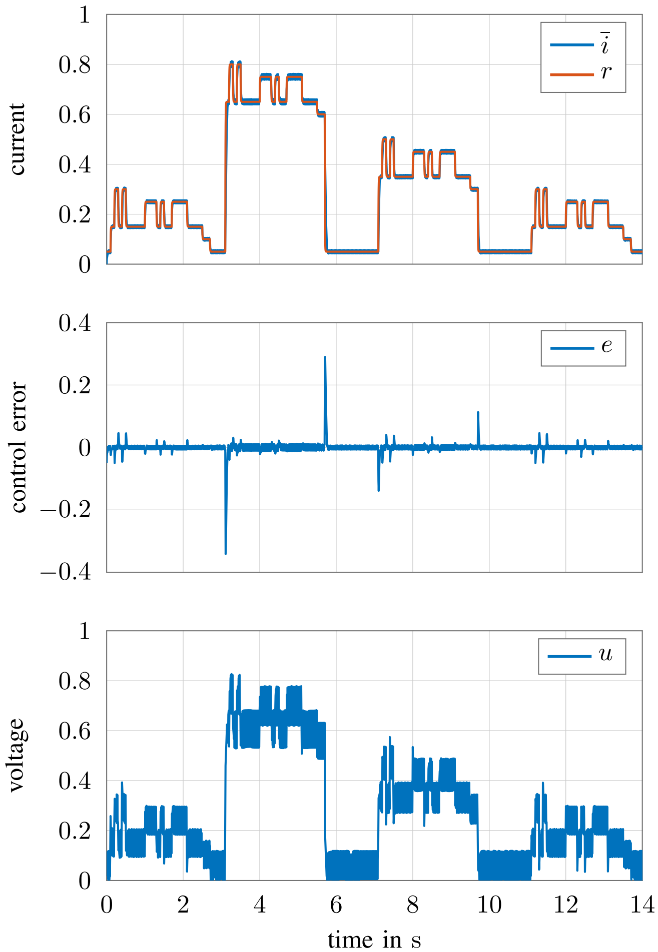

Fig. 4. Experimental results of the sliding mode controller for solenoid A. The values are normalized to i_A and v_{bat}, respectively.

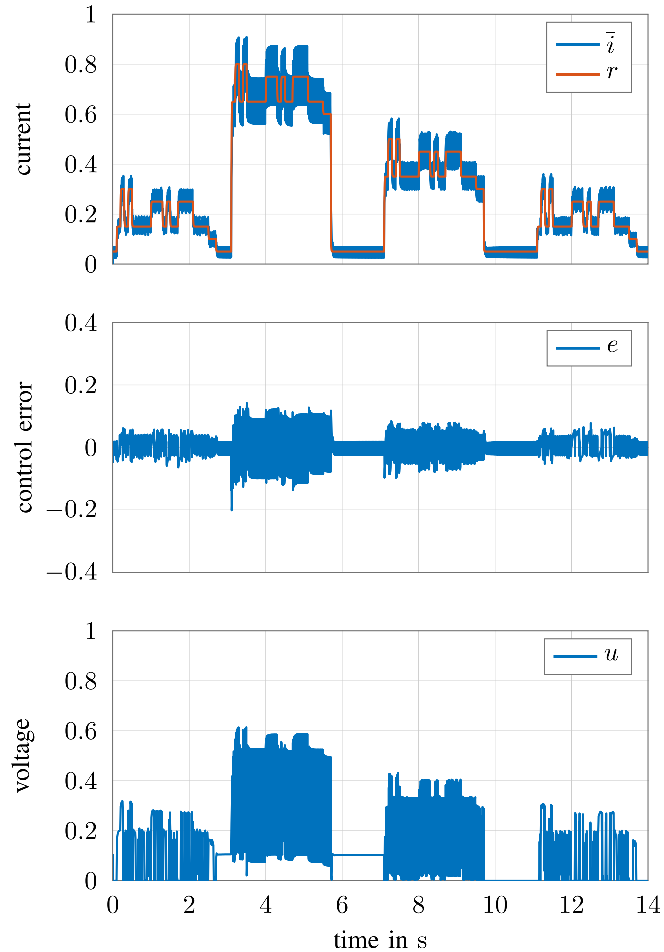

Fig. 5. Experimental results of the sliding mode controller for solenoid B. The values are normalized to i_A and v_{bat}, respectively.

B. Model Reference Adaptive Controller

As a benchmark for a well-known adaptive controller, the nonlinear model reference adaptive control scheme from [12], see also e.g., [34], is applied to (5), which yields

$$\dot{\boldsymbol{\vartheta}} = -\lambda \begin{bmatrix} y \\ \hat{R}y + \hat{L}(\dot{r} + K_p e) \end{bmatrix} e \tag{22a}$$

$$u = \hat{R}y + \hat{L}(\dot{r} + K_p e) \tag{22b}$$

with the control error $e = r - y$, the parameter estimate vector (see Remark 2)

$$\boldsymbol{\vartheta}^{\mathrm{T}} = \begin{bmatrix} 1/\hat{L} & \hat{R}/\hat{L} \end{bmatrix} \tag{23}$$

and the constant tuning coefficients $K_p > 0$ and $\lambda > 0$, respectively. The control law (22b) consists of a feedforward part using the time derivative of the reference signal $\dot{r}$, a static compensation of the estimated voltage caused by the resistance of the solenoid, and a proportional control term. As stated in the introduction, the control law is typically augmented by an adaptation algorithm to guarantee a decreasing Lyapunov function. Here, the commonly used quadratic functions lead to a gradient-type adaptation law. Note, however, that in this case the adaptation (22a) is driven by the control error e, rather than the estimation error ε.

VI. Experimental Validation

In this section, experimental results of the benchmark control approaches from Section V are presented and compared with the adaptive control scheme proposed in this article. For this purpose, three different solenoids, henceforth referred to as solenoids A, B, and C, are used for the experiments, see Fig. 3. The nominal current of solenoid A is denoted by i_A.

The three solenoids were taken from different fields of application and feature different mechanical and electromagnetic designs. In particular, solenoid A is used in a pressure control valve, solenoid B is part of a pilot valve of a hydraulic two-stage valve, and solenoid C is employed in an automatic transmission gear. Hence, there are significant differences in their nominal resistance and inductance parameters. Their nominal parameter values are given in Table I.

All experiments were conducted on a dSpace MicroLab Box at a sampling time of $T_s = 1\,\text{ms}$ and a modulation

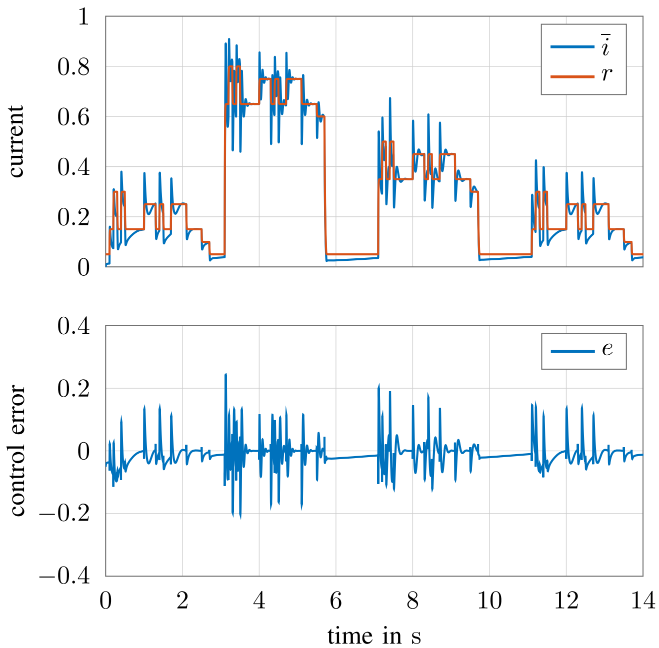

Fig. 6. Experimental results of the nonlinear model reference adaptive control scheme for solenoid A. The values are normalized to i_A.

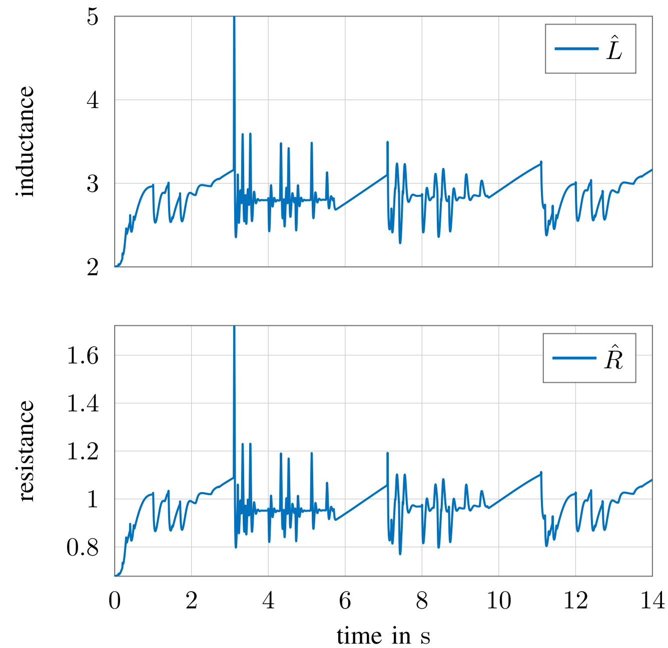

Fig. 7. Estimated parameters of the nonlinear model reference adaptive control scheme for solenoid A. The values are normalized to L_A and R_A, respectively.

period of $T_{\mathrm{pwm}} = 50\,\mu$m. The current is sampled at a rate of 10 μs and averaged over 100 measurements in order to mitigate the effects of the current ripple caused by switching the transistor. The battery voltage v_{bat} is used with a calibrated power electronics circuit to generate the PWM voltages across the solenoid terminals.

A. SMC Experiments

In this section, experimental results of the SMC law from [6], as outlined in Section V-A, are presented as a baseline for comparing the proposed method with a common approach in solenoid control. Figs. 4 and 5 show the experimental results achieved by the control input (21a) applied to the solenoids A and B. The tuning parameters are listed in Table II for both cases.

The peaks in the current error at 3.1 and 5.7 s in Fig. 4 are a consequence of the lack of a feedforward part in this control approach. This leads to a significant delay between the reference and the controlled current, which causes large control errors. The general performance of the well-tuned sliding mode controller for solenoid A, however, is very good. In contrast, Fig. 5 shows the experimental result for the same sliding mode controller applied to solenoid B. Even though the sliding mode controller is a robust control approach, the control performance is severely degraded by the poor tuning for this solenoid. In particular, the smaller inductance results in overshoots and persistent oscillations of the current. Furthermore, the nonlinearity of the solenoid inductance leads to a larger control error at higher current levels. It becomes clear from Figs. 4 and 5 that the sliding mode controller provides good results when properly tuned, but the performance may degrade significantly if retuning is not possible.

B. Model Reference Adaptive Control Experiments

In this section, experimental results of the nonlinear model reference adaptive control scheme from [12], as outlined in Section V-B, are presented. Fig. 6 shows the solenoid current and the control error of the algorithm from (22a) and (22b) applied to solenoid A. The tuning parameters used in the experiment can be found in Table III. The nominal parameters of the solenoid are given in Table I. The reference trajectory was selected to show the performance of the algorithm for rapid setpoint changes and for periods with insufficient excitation. During these periods at about 6 and 10 s the reference signal is constant, hence, the inductance and the resistance cannot be identified simultaneously. Additionally, the inductance varies significantly with the different current levels of the reference signal. This current- and position-dependence of the inductance is an unmodeled nonlinear effect. The current trajectory in Fig. 6 clearly shows that the adaptation algorithm cannot estimate the inductance and the resistance of the solenoid to achieve a satisfactory tracking performance. During periods of low excitation, the gradient-based adaptation law only converges slowly. Hence, in a steady state, the control error is slowly reduced, but the reference is not reached even after 1 s. The control error shows a large mean error with peaks over 0.2 i_A. Furthermore, the repeating reference signal at 11 s is not improved as compared to the tracking performance with the initial parameters at 0.1 s. Both cases show a peak error of 0.15 i_A.

Fig. 7 shows the estimated parameters of this experiment. Note that according to (22a), the parameter vector is updated proportionally to the control error. Hence, large control errors are necessary for the parameters to converge, which makes this

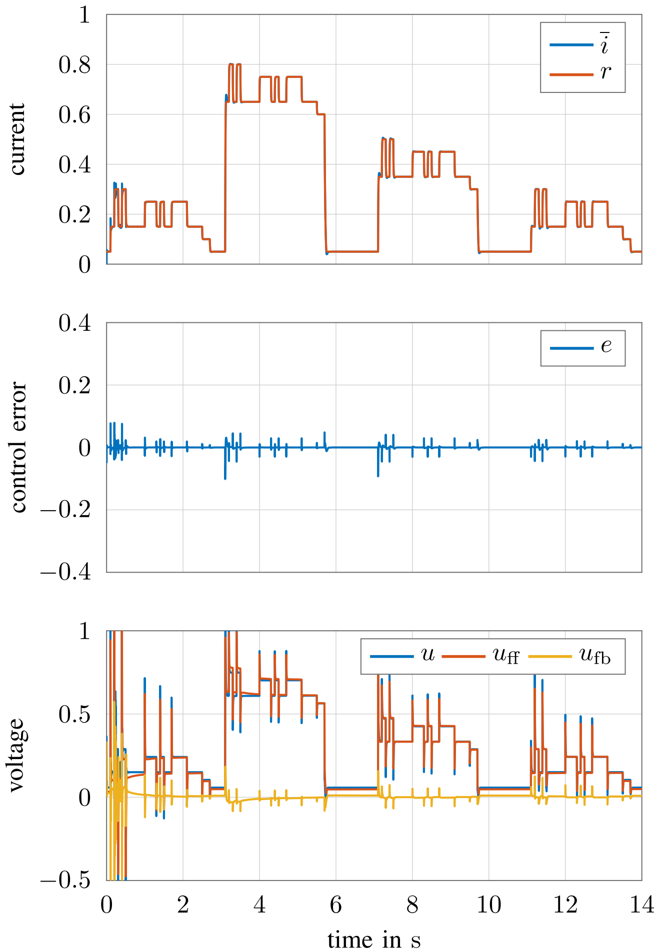

Fig. 8. Experimental results of the indirect adaptive two-degrees-of-freedom control algorithm for solenoid A. The values are normalized to i_A and v_{bat}, respectively.

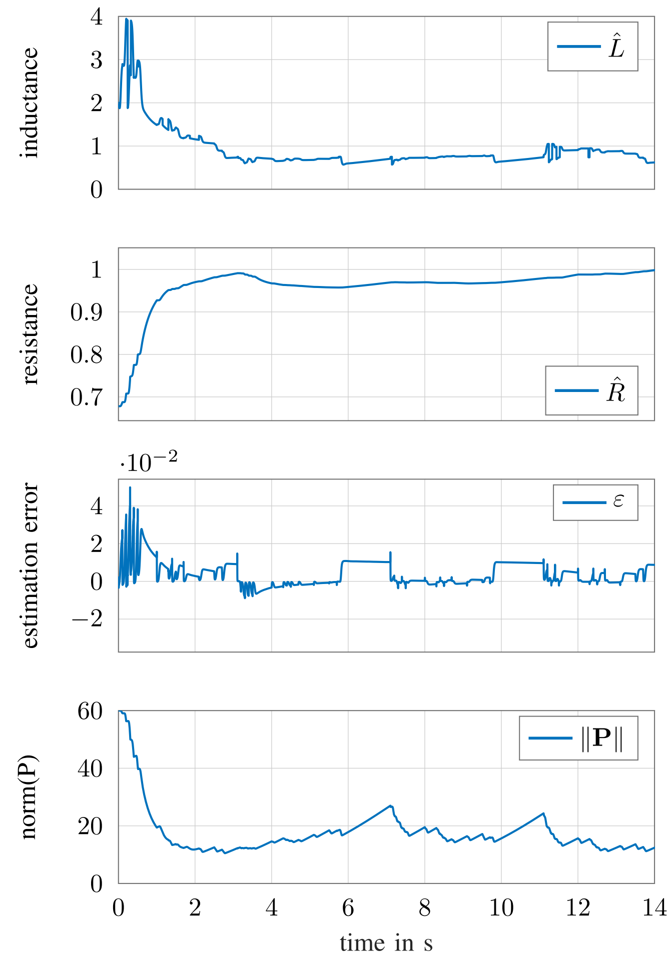

Fig. 9. Parameter estimates of the indirect adaptive two-degrees-of-freedom control algorithm for solenoid A. The values are normalized to L_A, R_A, and v_{bat}, respectively.

TABLE III

PARAMETERS USED FOR THE NONLINEAR MODEL REFERENCE ADAPTIVE CONTROL EXPERIMENT

Control & adaptation		Initial conditions	
K_p	10	$\hat{R}_0$	$0.68R_A$
λ	20	$\hat{L}_0$	$2.0L_A$

approach sensitive to model uncertainties such as the nonlinear inductance effects. Furthermore, the parameter update has a constant gain λ. These two properties lead to a fluctuating update of the estimated parameters and rapid changes, whenever a large control error occurs. The estimated inductance values and the lack of dynamic feedback lead to high current overshoots.

As discussed in Section III-A, projection bounds cannot be formulated tightly for the coupled parameter vector (23) which leads to estimates exceeding the desired bounds $L_{\max}$ and $R_{\max}$. At 3 s the resistance exceeds the desired bound of $R_{\max} = 1.36\ R_A$. During periods of low excitation at 6 and 10 s both parameters are used by the algorithm to counteract the steady-state error. During this time, however, only one independent parameter can be identified, i.e. there is no persistence of excitation. Hence, the parameters drift on a 1-D subspace of the parameter space. This drift is caused by the loss of observability of the parameters and methods such as the dead-zone have been proposed to mitigate the drift. However, it will be shown that the drift is much slower for the proposed method. Note that the estimated parameters strongly depend on the control error and therefore exhibit a very similar trajectory.

TABLE IV

PARAMETERS USED FOR THE EXPERIMENT WITH THE PROPOSED INDIRECT ADAPTIVE CONTROLLER

Control		Adaptation		Projection	
$\alpha_0{}^*$	$10\,000\,\mathrm{s}^{-2}$	L_0	$2.0L_A$	$L_{\min}$	$0.2L_A$
$\alpha_1{}^*$	$100\,\mathrm{s}^{-1}$	R_0	$0.68R_A$	$L_{\max}$	$5.0L_A$
		λ_a	$0.2\,\mathrm{s}^{-1}$	$R_{\min}$	$0.34R_A$
		P_0	60	$R_{\max}$	$1.36R_A$
		$\beta_{\max}$	0.6		
		$P_{\max}$	150		

C. Proposed Indirect Adaptive Control Scheme

In this section, the proposed indirect adaptive two-degrees-of-freedom control strategy is experimentally validated for all three investigated solenoids. To this end, the controller is

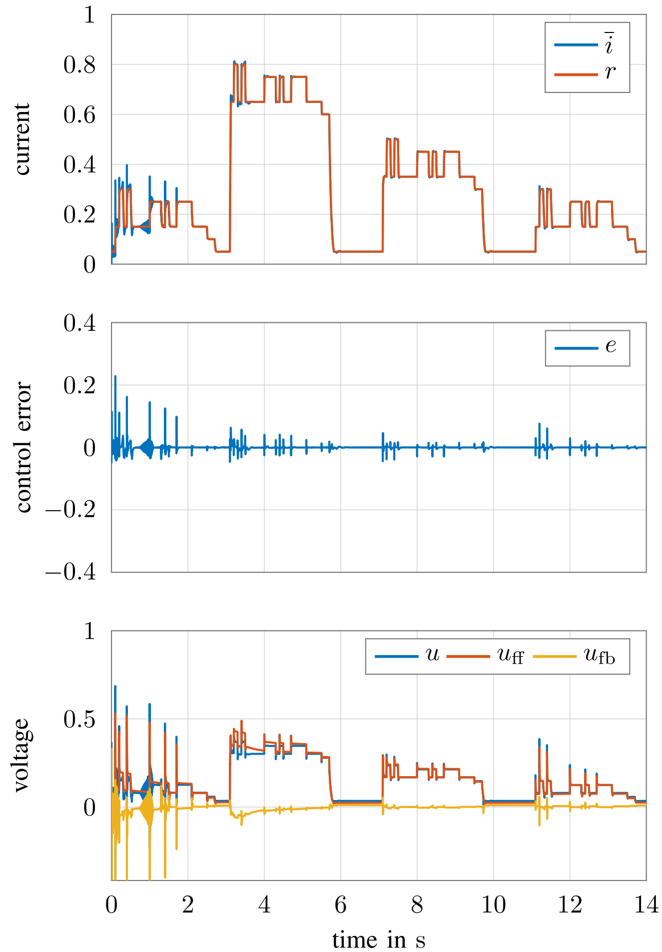

Fig. 10. Control signals of the indirect adaptive two-degrees-of-freedom control algorithm for solenoid B. The values are normalized to i_A and v_{bat}, respectively.

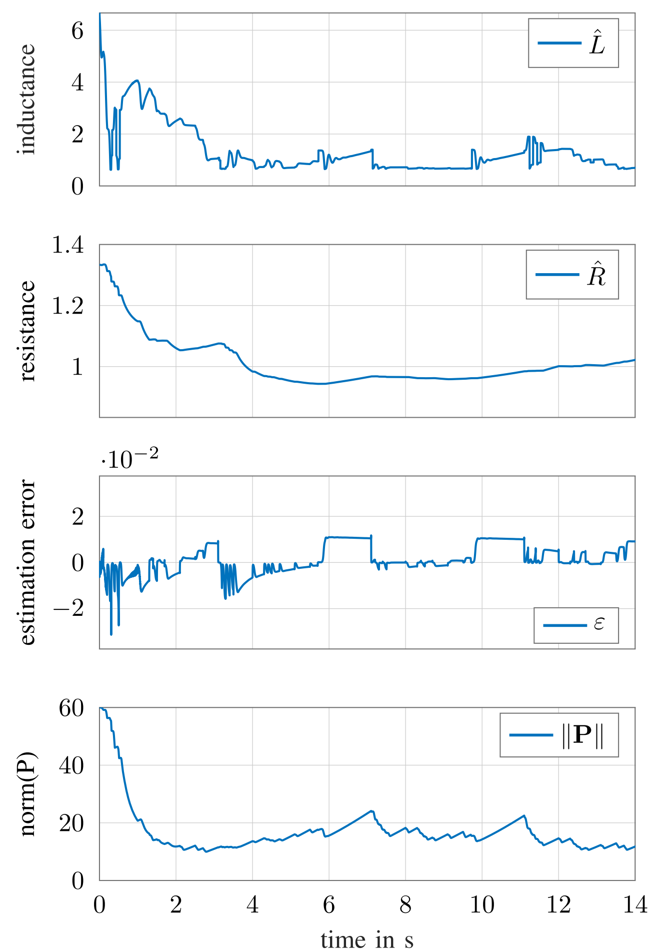

Fig. 11. Parameter estimates of the indirect adaptive two-degrees-of-freedom control algorithm for solenoid B. The values are normalized to L_B, R_B, and v_{bat}, respectively.

initialized with the same parameters for all three solenoids depicted in Fig. 3. The constrained forgetting least-squares adaptation algorithm in (14) was discretized following [13], [35], [36] as detailed in Appendix B. The control parameters and initial values can be found in Table IV. The controller parameters α_0^* and α_1^* were chosen for a time constant of 10 ms and a damping ratio of 0.5 for the closed-loop error system (20). The initial parameters R_0 and L_0 were set to typical nominal values within the parameter range of the considered solenoids. The time constant λ_a of the low-pass filter (6) is essentially determined by the measurement noise when calculating the time derivative of the current y. The initial and maximum gain matrix, P_0 and $P_{\max}$, and the forgetting factor $\beta_{\max}$ were tuned according to the procedure presented in [18] and can be treated similar to the classical least-squares tuning factors. The bounds for the inductance estimate, $L_{\min}$ and $L_{\max}$, and for the resistance estimate, $R_{\min}$ and $R_{\max}$, reported in Table IV, are selected to restrict the parameters to physically meaningful values. These bounds do not influence the transient performance of the overall algorithm.

In direct comparison with the MRC and the SMC scheme, Fig. 8 shows experimental results of the indirect adaptive control algorithm (14)–(19) applied to solenoid A. Here, the control error decays quickly after an initial convergence of the estimated plant parameters. The large contribution of the feedforward controller u_{ff} to the overall control input u suggests that the parametrized model accurately describes the physical plant. Hence, the feedback controller is used around the reference trajectory and can be tuned independently of the reference tracking control task. The repeated pattern of the reference signal at 11 s underlines the improvement of the control performance achieved by the adaptation. Here, the control performance is significantly improved compared to the reference signal controlled using the initial parameters at 0.1 s. At 3 s the feedback controller shows an increased activity caused by the high current, which entails a decrease in the inductance. This effect is compensated by the feedback controller and does not significantly impact the control performance. Hence, the interaction between adaptation and integral feedback control combines fast convergence of the parameters with robustness to model uncertainties and unmodeled effects. Additionally, the least-squares adaptation algorithm from (14) uses the estimation error and can be adapted even without a control error. Thus, control errors due to disturbances are compensated by the feedback controller,

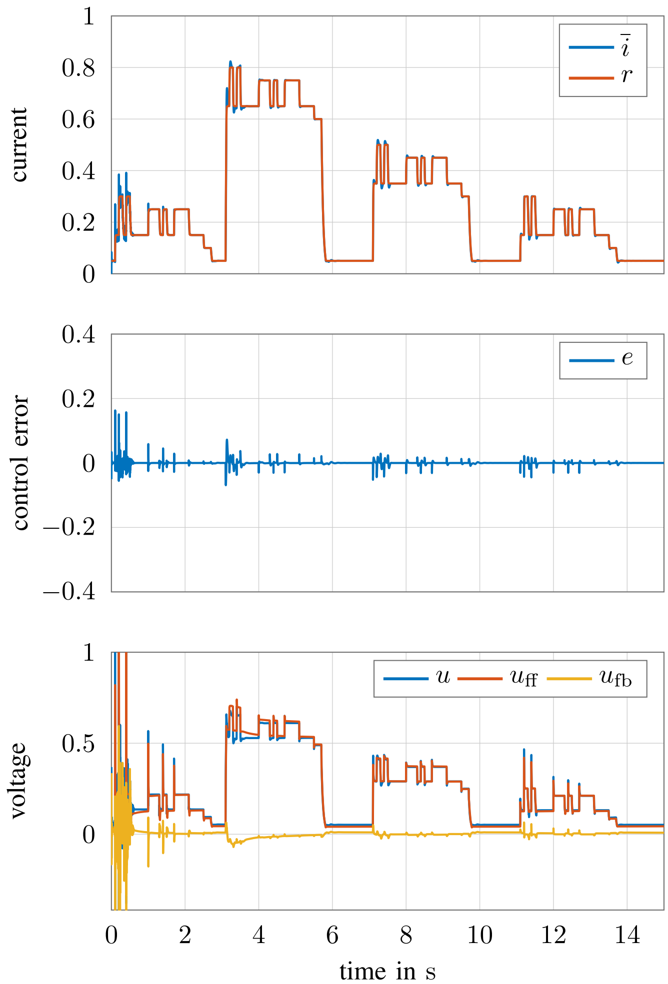

Fig. 12. Control signals of the indirect adaptive two-degrees-of-freedom control algorithm for solenoid C. The values are normalized to i_A and v_{bat}, respectively.

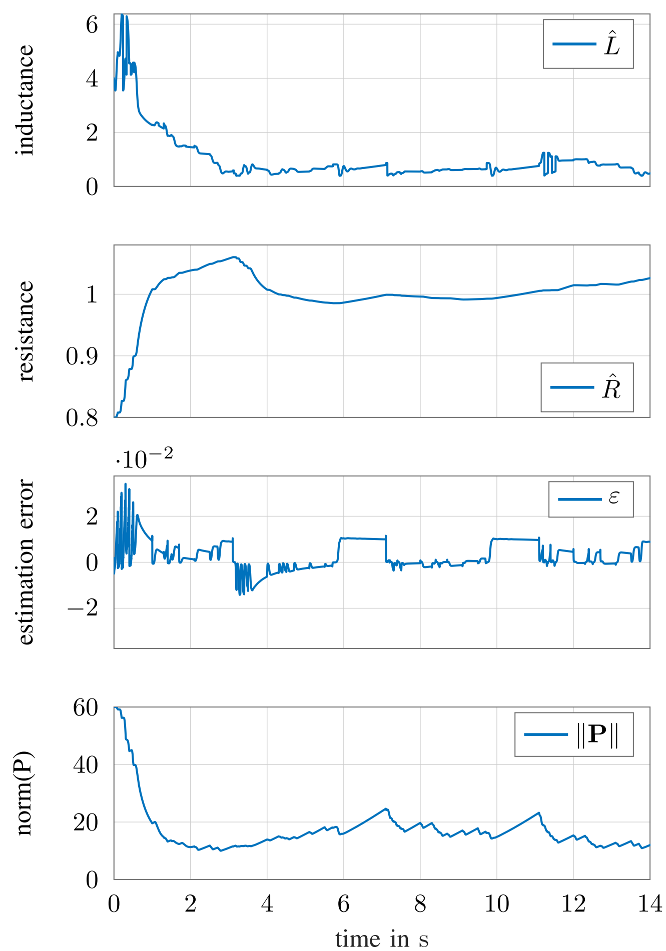

Fig. 13. Estimated parameters of the indirect adaptive two-degrees-of-freedom control algorithm for solenoid C. The values are normalized to L_C, R_C, and v_{bat}, respectively.

whereas the parameters are updated when an estimation error occurs.

The estimated parameters, the normalized estimation error (11) and the norm of the gain matrix are depicted in Fig. 9. The large estimation error and gain matrix norm in the first second of the experiment leads to a rapid convergence of the resistance and inductance estimates. The high initial gain value is used to reduce the estimation error quickly, while after this convergence phase the gain matrix of the estimation algorithm (14) adapts to the current excitation. During periods of low excitation at 6 and 10 s, the gain matrix is increased again by the exponential forgetting. Hereby, any parameter errors accumulated during this period are rapidly compensated for as soon as the parameters are excited again, as indicated by the estimation error. In contrast, a least-squares algorithm without exponential forgetting cannot neglect faulty measurements, even if new correct data is collected afterward. Furthermore, the estimated parameters show only negligible drift in the steady state. In applications with long periods of insufficient excitation, modifications like a dead zone can be added to account for the lack of excitation in the reference signal, see, e.g., [11].

Solenoid B has approximately half the resistance and a drastically smaller inductance, as compared to solenoid A. However, Fig. 10 shows that the adaptation algorithm of the *same* controller as the one used for solenoid A applied to solenoid B rapidly converges and establishes a small control error throughout the whole reference trajectory. Here, again, the nonlinear effect of the change in inductance at 3 s is compensated by the feedback control term u_{fb}. The feedforward part already achieves precise reference tracking after the initial convergence period. This is illustrated by the small feedback control action $u_{\mathbf{fb}}$ after about 5 s. Thereafter, the control error stays well below 0.1 i_A even with rapid changes in the reference signal and periods of low excitation. Caused by the strong deviations of the initial conditions of the parameters from the real values, the controller shows some overshoots until the parameters have converged. Similar to the results with solenoid A, the parameters quickly converge and after 3 s excellent tracking performance and a low control error are achieved, see Fig. 11. The experimental results for solenoid C are depicted in Fig. 12. The large initial value of the estimated inductance parameter causes overshoots during the first second of the experiment and around 3 s due to the nonlinear inductance. However, from Fig. 13 it can be seen that the inductance estimate decreases and eventually leads to excellent control performance. Furthermore, it should be noted that the estimated resistance parameter changes between 3 and 4 s, due to the excitation of the reference signal. The small feedback control action u_{fb}, again, shows a good match between the adaptively parametrized model and the controlled solenoid after the initial convergence phase.

VII. Conclusion

An indirect adaptive two-degrees-of-freedom control algorithm for the current control of solenoids is proposed. The contribution of this article is threefold. First, the indirect adaptive pole placement scheme known from the literature is extended by an adaptive feedforward part and the formulation is modified to improve its robustness. A thorough stability proof is provided for the overall closed-loop system comprising the plant, the constrained bounded-gain forgetting least-squares parameter estimation scheme, and the adaptive two-degrees-of-freedom control concept, both described in detail in Section III. For rapidly changing reference trajectories, the adaptive feedforward part turns out to essentially improve the tracking performance also for time-varying parameters. The constrained bounded-gain forgetting least-squares parameter estimation scheme ensures fast convergence of the parameters and does not suffer from excessive drift during periods of low excitation. Since the control design model does not account for the nonlinearity of the inductance and the time-varying parameters, the derived stability proof does not ensure stability for the nonlinear plant (4). However, the achieved closed-loop control performance in the experiments justifies the proposed approach.

Further research is to be conducted to improve the parameter convergence in situations of low excitation, which is an active field of research, see, e.g., [28]. The proposed adaptive control scheme strongly benefits from its property that the control error convergence does not rely on the convergence of the parameters. This alleviates the need for the persistence of the excitation assumption and yields a good control performance without the persistence of excitation in the presented experiments.

The second contribution of this article refers to experimental validation. The feasibility and the good performance of the proposed approach are demonstrated by applying the control concept with one nominal controller tuning to three different solenoids from various applications, with strongly differing parameters. Thus, for a whole range of different solenoids, only a single controller tuning is required and the proposed adaptation scheme shows a robust and high-performance operation without further adjustments. This saves time and costs, in particular during commissioning, and ensures high performance also under changing loads and environmental conditions.

As a third point, experimental results of the performance of the proposed solution are compared with two well-known benchmark methods for solenoid control, taken from the literature, i.e. a robust second-order sliding-mode controller and a nonlinear model reference adaptive control approach. The sliding mode controller requires retuning for every solenoid and the model reference adaptive controller exhibits a poor adaptation performance.

Appendix

A. Proof of Theorem 2

The proof proceeds similar to the proof presented in [11, p. 471]. However, there are essential differences from the original proof, such as the integral feedback path, the feedforward controller, and the formulation of the least-squares problem. Therefore in the following, the main aspects of the proof are sketched.

The filtered system input and output can be written with (7) as

$$\dot{u}_a = -\lambda_a u_a + \lambda_a u \quad u_a(0) = u_0 \tag{24a}$$
$$\dot{y}_a = -\lambda_a y_a + \lambda_a y \quad y_a(0) = y_0 \tag{24b}$$

with initial conditions u_0 and y_0.

Consequently, the least-squares estimation error is given by, cf. (11)

$$\varepsilon = \frac{u_a - \hat{L}\dot{y}_a - \hat{R}y_a}{m^2} \tag{25}$$

with the normalization factor $m^2 = 1 + y_a^2 + \dot{y}_a^2$ and the estimated parameters $\hat{L}$ and $\hat{R}$. In addition, the control input from (19) can be written as

$$u = \hat{k}_p(r - y) + \hat{k}_i x_c + \hat{L}\dot{r} + \hat{R}r \tag{26}$$

with the integral control error x_c from (15b). The reference trajectory has to be chosen such that $r, \dot{r} \in \mathcal{L}_\infty$, which is satisfied by the assumptions in Section IV.

The proof of Theorem 2 is performed in the four steps listed in Section IV. Rearrangement of (24), (25), and (26) yield the system

$$\dot{\boldsymbol{\psi}} = \mathbf{A}(t)\boldsymbol{\psi} + \mathbf{b}_1(t)\varepsilon m^2 + \mathbf{b}_2(t)r + \mathbf{b}_3(t)\dot{r} \tag{27}$$

where

$$\boldsymbol{\psi} = \begin{bmatrix} u_a \\ y_a \\ x_c \end{bmatrix}, \quad \mathbf{b}_1(t) = \frac{1}{\hat{L}}\begin{bmatrix} \hat{k}_p \\ -1 \\ \frac{1}{\lambda_a} \end{bmatrix} \tag{28}$$

$$\mathbf{b}_2(t) = \begin{bmatrix} \lambda_a\left(\hat{k}_p + \hat{R}\right) \\ 0 \\ 1 \end{bmatrix}, \quad \mathbf{b}_3(t) = \begin{bmatrix} \lambda_a\hat{L} \\ 0 \\ 0 \end{bmatrix} \tag{29}$$

and

$$\mathbf{A}(t) = \begin{bmatrix} -\lambda_a - \frac{\hat{k}_p}{\hat{L}} & -\lambda_a\hat{k}_p + \frac{\hat{R}}{\hat{L}}\hat{k}_p & \lambda_a\hat{k}_i \\ \frac{1}{\hat{L}} & -\frac{\hat{R}}{\hat{L}} & 0 \\ -\frac{1}{\lambda_a\hat{L}} & \frac{\hat{R}}{\hat{L}\lambda_a} - 1 & 0 \end{bmatrix}. \tag{30}$$

The input and output of the plant can be written as an output of this system by substituting (27) into (24a), and (24b), yielding

$$\begin{bmatrix} u \\ y \end{bmatrix} = \mathbf{C}(t)\boldsymbol{\psi} + \mathbf{d}_1(t)\varepsilon m^2 + \mathbf{d}_2(t)r + \mathbf{d}_3(t)\dot{r} \tag{31}$$

with the output matrix and vectors

$$\mathbf{C}(t) = \begin{bmatrix} -\frac{\hat{k}_p}{\lambda_a \hat{L}} & \frac{\hat{k}_p \hat{R}}{\lambda_a \hat{L}} - \hat{k}_p & \hat{k}_i \\ \frac{1}{\lambda_a \hat{L}} & 1 - \frac{\hat{R}}{\lambda_a \hat{L}} & 0 \end{bmatrix}, \quad \mathbf{d}_1(t) = \begin{bmatrix} \frac{\hat{k}_p}{\lambda_a \hat{L}} \\ -\frac{1}{\lambda_a \hat{L}} \end{bmatrix} \tag{32}$$

$$\mathbf{d}_2(t) = \begin{bmatrix} \hat{R} + \hat{k}_p \\ 0 \end{bmatrix}, \quad \mathbf{d}_3(t) = \begin{bmatrix} \hat{L} \\ 0 \end{bmatrix}. \tag{33}$$

Due to the projection the adaptation algorithm (14) ensures that $\hat{R}$ and $\hat{L}$ are bounded from below and above. In particular $0 < L_{\min} \leq \hat{L}$, which guarantees that $\mathbf{A}(t), \mathbf{b}_i(t), \mathbf{C}(t)$, and $\mathbf{d}_i(t)$ $i = 1, 2, 3$ are bounded.

Next, it will be shown that the homogeneous part of (27) is exponentially stable. This will be done by showing that the eigenvalues of $\mathbf{A}(t)$, for all times t, are negative and the induced norm $\|\dot{\mathbf{A}}(t)\| \in \mathcal{L}_2$. The characteristic polynomial of $\mathbf{A}(t)$ reads as

$$\det\Big(\mathbf{A}(t) - s\mathbf{I}\Big) = \big(s + \lambda_a\big)\Big(s^2 + \alpha_1^* s + \alpha_0^*\Big). \tag{34}$$

Thus, the first pole of the system is determined by the filter of the adaptation algorithm and the remaining two poles by the desired closed-loop dynamics. If the poles of (20) are chosen to be in the open left half-plane and $\lambda_a > 0$, then the eigenvalues of $\mathbf{A}(t)$ have a negative real part for all times t.

According to Theorem 1, $\hat{L}, \dot{\hat{L}}, \hat{R}, \dot{\hat{R}} \in \mathcal{L}_\infty$ and $\dot{\hat{L}}, \dot{\hat{R}} \in \mathcal{L}_2$. This together with the bound $0 < L_{\min} \leq \hat{L}$, which is guaranteed by the projection (14), implies that $\|\dot{\mathbf{A}}(t)\| \in \mathcal{L}_\infty \bigcap \mathcal{L}_2$. Thus, based on [11, Th. 3.4.11, p. 124] the homogeneous part of (27) is exponentially stable.

In the next step, these results are used to establish boundedness of the system signals using the truncated exponentially weighted $\mathcal{L}_{2\delta}$ norm and the Bellman-Gronwall Lemma. Here, the procedure is similar to what is shown in [11, p.472]. Thus, by applying the Bellmann-Gronwall Lemma [11, Lemma 3.3.9, p. 103] we conclude that $m, y_a, \dot{y}_a \in \mathcal{L}_\infty$, for all times $t > 0$. Substituting into (25) and using $\varepsilon \in \mathcal{L}_\infty$ (by Theorem 1) leads to $u_a \in \mathcal{L}_\infty$. It then follows that $\boldsymbol{\psi}, \dot{\boldsymbol{\psi}}, y, u \in \mathcal{L}_\infty$.

In the last step, the convergence of the control error will be addressed. Here, the parameter estimator properties, the boundedness of the system signals, and the plant dynamics are used to prove the convergence of the control error by using Barbalat's lemma. Given a vector signal $t \mapsto a(t) \in \mathbb{R}^n$ filtered componentwise by an LTI filter with the transfer function $W(s)$, we denote by $W[a]$ the corresponding output signal. With this notation, the following lemma is a corollary of the swapping lemma [11, Lemma A.1, p. 774].

Lemma 1: Given a stable proper transfer function $W(s)$ and two differentiable signals $t \mapsto a(t)$ and $t \mapsto b(t)$ such that $b \in \mathcal{L}_\infty$ and $\dot{a} \in \mathcal{L}_\infty \bigcap \mathcal{L}_2$, there exists a signal $\rho \in \mathcal{L}_\infty \bigcap \mathcal{L}_2$ such that

$$W\Big[a^{\mathrm{T}} b\Big] = a^{\mathrm{T}} W\Big[b\Big] + \rho. \tag{35}$$

Using the aforementioned assumptions and theorems the estimation error equation will now be bounded. Rearranging (25) and taking the time derivative results in

$$\begin{aligned} \frac{\mathrm{d}}{\mathrm{d}t}\Big(\varepsilon m^2\Big) &= \dot{u}_a - \frac{\mathrm{d}}{\mathrm{d}t}\Big(\hat{L}\dot{y}_a + \hat{R} y_a\Big) \\ &= \dot{u}_a - \hat{L}\ddot{y}_a - \hat{R}\dot{y}_a + \rho_1 \end{aligned} \tag{36}$$

with the rest term $\rho_1 \in \mathcal{L}_\infty \bigcap \mathcal{L}_2$. Application of the filter

$$W = \frac{\lambda_a s}{s + \lambda_a} \tag{37}$$

to (26) yields

$$\dot{u}_a = W\left[\Big[\hat{L} \ \hat{R}\Big]\begin{bmatrix} \dot{r} \\ r \end{bmatrix}\right] + W\left[\Big[\hat{k}_p \ \hat{k}_i\Big]\begin{bmatrix} e \\ x_c \end{bmatrix}\right]. \tag{38}$$

Rewriting this expression using Lemma 1 yields

$$\dot{u}_a = \Big[\hat{L} \ \hat{R}\Big] W\left[\begin{bmatrix} \dot{r} \\ r \end{bmatrix}\right] + \Big[\hat{k}_p \ \hat{k}_i\Big] W\left[\begin{bmatrix} e \\ x_c \end{bmatrix}\right] + \rho_2 + \rho_3 \tag{39}$$

with $\rho_2, \rho_3 \in \mathcal{L}_\infty \bigcap \mathcal{L}_2$. Substituting (39) into (36) and using (17) gives

$$\frac{\mathrm{d}}{\mathrm{d}t}\Big(\varepsilon m^2\Big) = \hat{L} A^* \Lambda_a e + \bar{\rho} \tag{40}$$

where $A^* = (\mathrm{d}/\mathrm{d}t)^2 + \alpha_1^*(\mathrm{d}/\mathrm{d}t) + \alpha_0^*$ refers to the desired pole-placement polynomial, see (20), and $\bar{\rho} = \sum_{i=1}^{3} \rho_i \in \mathcal{L}_\infty \bigcap \mathcal{L}_2$. Rearranging for the control error e and using the product rule yields

$$e = \frac{1}{\Lambda_a A^*}\left(\frac{\mathrm{d}}{\mathrm{d}t}\left(\frac{1}{\hat{L}}\varepsilon m^2\right) + \frac{\dot{\hat{L}}}{\hat{L}^2}\varepsilon m^2 - \frac{\bar{\rho}}{\hat{L}}\right). \tag{41}$$

Since $\hat{L} \in \mathcal{L}_\infty$ as well as $\dot{\hat{L}}, \varepsilon m^2 \in \mathcal{L}_\infty \bigcap \mathcal{L}_2$, and $A^*(s)$ is a Hurwitz polynomial by design, it follows that $e \in \mathcal{L}_\infty \bigcap \mathcal{L}_2$. Additionally from a special case of Barbalat's lemma [11, Lemma 3.2.5, p. 76] it follows that $\dot{e} \in \mathcal{L}_\infty$ and

$$\lim_{t \to \infty} e(t) = 0. \tag{42}$$

We will now show that the parameter rates converge to zero. Equation (36) can be expanded to

$$\frac{\mathrm{d}}{\mathrm{d}t}\Big(\varepsilon m^2\Big) = \dot{u}_a - \dot{\hat{L}}\dot{y}_a - \hat{L}\ddot{y}_a - \dot{\hat{R}} y_a - \hat{R}\dot{y}_a. \tag{43}$$

Due to (6) $\ddot{y}_a \in \mathcal{L}_\infty$ holds and since $\boldsymbol{\psi}, \dot{\boldsymbol{\psi}}, \hat{R}, \hat{L}, \dot{\hat{R}}, \dot{\hat{L}} \in \mathcal{L}_\infty$, it can be concluded that $(\mathrm{d}/\mathrm{d}t)(\varepsilon m^2) \in \mathcal{L}_\infty$. This together with $\varepsilon m^2 \in \mathcal{L}_\infty \bigcap \mathcal{L}_2$ and the uniform continuity of (43) leads via Barbalat's Lemma to $\varepsilon m^2 \to 0$, as $t \to \infty$. Because $m^2 \geq 1$, it can be further concluded that $\varepsilon \to 0$ as $t \to \infty$. By using the structure of the estimator in (14) and since the gain matrix $\mathbf{P} \in \mathcal{L}_\infty$, it can be concluded that $\dot{\hat{R}}, \dot{\hat{L}} \to 0$ as $t \to \infty$. It follows from (17) that $\dot{\hat{k}}_i \to 0$ and $\dot{\hat{k}}_p \to 0$ as $t \to \infty$. This concludes the proof.

Remark 4: It is guaranteed that the estimation error ε and the plant and control parameter rates $\dot{\hat{R}}, \dot{\hat{L}}, \dot{\hat{k}}_p, \dot{\hat{k}}_i$ converge to zero. It is not guaranteed that the plant and control parameters $\hat{R}, \hat{L}, \hat{k}_p, \hat{k}_i$ will converge to the true values of $\bar{R}, \bar{L}, \bar{k}_p, \bar{k}_i$. Indeed it is not ensured that the signals used in the estimation algorithm are persistently exciting.

B. Discrete-Time Constrained Bounded-Gain Forgetting Least-Squares Algorithm

Next, the discrete-time implementation of the constrained bounded-gain forgetting least-squares algorithm from Section III-A is summarized. We apply a time discretization for $t = kT_s$ with the sampling time T_s and $k \in 1, 2, \ldots, N$. Subsequently, the index k refers to the sampling instant at time kT_s, i.e. $f_k = f(kT_s)$. For the given application, we consider box constraints of the form

$$\mathcal{S} = \left[L_{\min}, L_{\max}\right] \times \left[R_{\min}, R_{\max}\right] \tag{44}$$

with lower limits $L_{\min}$ and $R_{\min}$ and upper limits $L_{\max}$ and $R_{\max}$. In this case, an analytical solution to the orthogonal projection of (12) is given by

$$\mathcal{P}_{\vartheta}\left(\boldsymbol{\vartheta}\right) = \begin{bmatrix} \mathcal{P}_L\left(\hat{L}\right) \\ \mathcal{P}_R\left(\hat{R}\right) \end{bmatrix} \tag{45}$$

with

$$\mathcal{P}_L\left(\hat{L}_{k+1}\right) = \begin{cases} L_{\min}, & \text{if } \hat{L}_{k+1} < L_{\min} \\ L_{\max}, & \text{if } \hat{L}_{k+1} > L_{\max} \\ \hat{L}_{k+1}, & \text{if } L_{\min} \leq \hat{L}_{k+1} \leq L_{\max} \end{cases} \tag{46}$$

and

$$\mathcal{P}_R\left(\hat{R}_{k+1}\right) = \begin{cases} R_{\min}, & \text{if } \hat{R}_{k+1} < R_{\min} \\ R_{\max}, & \text{if } \hat{R}_{k+1} > R_{\max} \\ \hat{R}_{k+1}, & \text{if } R_{\min} \leq \hat{R}_{k+1} \leq R_{\max}\,. \end{cases} \tag{47}$$

Hence, the parameters are constrained by using the Goldstein-Levitin-Polyak projection algorithm, see, e.g., [36]. The discrete-time constrained bounded-gain forgetting least-squares algorithm, with $\boldsymbol{\vartheta}_k = \boldsymbol{\vartheta}(kT_s)$ and $\mathbf{P}_k = \mathbf{P}(kT_s)$, reads as [35, p. 365] and [13, Chapter 3.7, p. 91]

$$\mathbf{L}_k = \frac{\mathbf{P}_{k-1}\boldsymbol{\varphi}_k}{\lambda_k + \boldsymbol{\varphi}_k^{\mathrm{T}}\mathbf{P}_{k-1}\boldsymbol{\varphi}_k} \tag{48a}$$

$$\mathbf{P}'_k = \frac{1}{\lambda_k}\left(\mathbf{P}_{k-1} - \mathbf{L}_k\boldsymbol{\varphi}_k^{\mathrm{T}}\mathbf{P}_{k-1}\right) \tag{48b}$$

$$\boldsymbol{\vartheta}_k = \mathcal{P}_{\vartheta}\left(\boldsymbol{\vartheta}_{k-1} + \mathbf{L}_k\left(z_k - \boldsymbol{\varphi}_k^{\mathrm{T}}\boldsymbol{\vartheta}_{k-1}\right)\right) \tag{48c}$$

$$\mathbf{P}_k = \Pi_p\left(\boldsymbol{\vartheta}_k, \mathbf{P}'_k\right) \tag{48d}$$

with the discrete-time forgetting factor

$$\lambda_k = 1 - T_s\beta_{\max}\left(1 - \frac{\|\mathbf{P}_k\|}{P_{\max}}\right) \tag{48e}$$

and the gain matrix projection operator

$$\Pi_p\left(\boldsymbol{\vartheta}_k, \cdot\right) = \begin{cases} \mathbf{P}'_k, & \text{if } \boldsymbol{\vartheta}_k \in \mathcal{S} \\ \mathbf{P}_{k-1}, & \text{otherwise.} \end{cases} \tag{48f}$$

References

[1] X. Zhao, L. Li, J. Song, C. Li, and X. Gao, "Linear control of switching valve in vehicle hydraulic control unit based on sensorless solenoid position estimation," *IEEE Trans. Ind. Electron.*, vol. 63, no. 7, pp. 4073–4085, Jul. 2016.

[2] L. Zhang, L. Liu, X. Zhu, and Z. Xu, "An electric load simulator for engine camless valvetrains," *Appl. Sci.*, vol. 9, no. 8, p. 1591, Apr. 2019.

[3] J. R. M. Van Dam, B. L. J. Gyser, M. Roes, and E. A. Lomonova, "Comparison of soft-landing position control and energy minimization performance of two fluid-control solenoid valves," in *Proc. Eur. Conf. Power Electron. Appl.*, 2018, pp. 1–9.

[4] B. Zardin, M. Borghi, G. Cillo, C. A. Rinaldini, and E. Mattarelli, "Design of two-stage on/off cartridge valves for mobile applications," *Energy Proc.*, vol. 126, pp. 1123–1130, Sep. 2017.

[5] K. Ma, D. Sun, G. Sun, Y. Kan, and J. Shi, "Design and efficiency analysis of wet dual clutch transmission decentralised pump-controlled hydraulic system," *Mechanism Mach. Theory*, vol. 154, Dec. 2020, Art. no. 104003.

[6] C. Krimpmann, G. Schoppel, I. Glowatzky, and T. Bertram, "Performance evaluation of nonlinear surfaces for sliding mode control of a hydraulic valve," in *Proc. IEEE Conf. Control Appl. (CCA)*, Sydney, NSW, Australia, Sep. 2015, pp. 822–827.

[7] K. Laib, A. R. Meghnous, M. T. Pham, and X. Lin-Shi, "Averaged state model and sliding mode observer for on/off solenoid valve pneumatic actuators," in *Proc. Amer. Control Conf. (ACC)*, Jul. 2016, pp. 4569–4574.

[8] S. Hodgson, M. Tavakoli, M. T. Pham, and A. Leleve, "Nonlinear discontinuous dynamics averaging and PWM-based sliding control of solenoid-valve pneumatic actuators," *IEEE/ASME Trans. Mechatronics*, vol. 20, no. 2, pp. 876–888, Apr. 2015.

[9] T. Braun, F. Strausberger, and J. Reuter, "State estimation for fast-switching solenoid valves: A study on practical nonlinear observers and new experimental results," in *Proc. 20th Int. Conf. Methods Models Autom. Robot. (MMAR)*, Aug. 2015, pp. 862–867.

[10] P. Ioannou, *Adaptive Control Tutorial* (Advances in Design and Control). Philadelphia, PA, USA: Society for Industrial and Applied Mathematics, 2006.

[11] P. A. Ioannou and J. Sun, *Robust Adaptive Control*. New York, NY, USA: Dover, 2012.

[12] S. Sastry and M. Bodson, *Adaptive Control: Stability, Convergence and Robustness* (Information and System Sciences). Upper Saddle River, NJ, USA: Prentice-Hall, 1989.

[13] G. C. Goodwin and K. S. Sin, *Adaptive Filtering Prediction and Control*. New York, NY, USA: Courier Corporation, 1984.

[14] M. Bin, L. Marconi, and A. R. Teel, "Results on adaptive output regulation for linear systems by least-squares identifiers," in *Proc. IEEE Conf. Decis. Control (CDC)*, Dec. 2018, pp. 1391–1396.

[15] I. Karafyllis and M. Krstic, "Adaptive certainty-equivalence control with regulation-triggered finite-time least-squares identification," *IEEE Trans. Autom. Control*, vol. 63, no. 10, pp. 3261–3275, Oct. 2018.

[16] M. S. Boroujeni, G. A. Markadeh, and J. Soltani, "Adaptive input-output feedback linearization control of brushless DC motor with arbitrary current reference using voltage source inverter," in *Proc. 8th Power Electron., Drive Syst. Technol. Conf. (PEDSTC)*, 2017, pp. 537–542.

[17] J.-J. E. Slotine and W. Li, *Applied Nonlinear Control*. Upper Saddle River, NJ, USA: Prentice-Hall, 1991.

[18] V. Shaferman, M. Schwegel, T. Glück, and A. Kugi, "Continuous-time least-squares forgetting algorithms for indirect adaptive control," *Eur. J. Control*, vol. 62, pp. 105–112, Nov. 2021.

[19] G. Pillonetto, A. Carè, and M. C. Campi, "Kernel-based SPS," in *Proc. Symp. Syst. Identificat.* Stockholm, Sweden: Elsevier, vol. 51, no. 15, 2018, pp. 31–36.

[20] Y. Sun, S. Oymak, and M. Fazel, "Finite sample system identification: Improved rates and the role of regularization," in *Proc. Mach. Learn. Res.*, vol. 120, 2020, pp. 1–10.

[21] S. Oymak and N. Ozay, "Non-asymptotic identification of LTI systems from a single trajectory," in *Proc. Amer. Control Conf. (ACC)*, Jul. 2019, pp. 5655–5661.

[22] B. C. Csáji, M. C. Campi, and E. Weyer, "Sign-perturbed sums: A new system identification approach for constructing exact non-asymptotic confidence regions in linear regression models," *IEEE Trans. Signal Process.*, vol. 63, no. 1, pp. 169–181, Nov. 2014.

[23] A. Carè, B. C. Csáji, M. C. Campi, and E. Weyer, "Finite-sample system identification: An overview and a new correlation method," *IEEE Control Syst. Lett.*, vol. 2, no. 1, pp. 61–66, Jan. 2017.

[24] M. Simchowitz, R. Boczar, and B. Recht, “Learning linear dynamical systems with semi-parametric least squares,” in *Proc. 32nd Conf. Learn. Theory*, in Proceedings of Machine Learning Research, vol. 99, A. Beygelzimer and D. Hsu, Eds. Phoenix, AZ, USA: PMLR, Jun. 2019, pp. 2714–2802. [Online]. Available: https://proceedings.mlr.press/v99/simchowitz19a.html

[25] G. Chowdhary and E. Johnson, “Least squares based modification for adaptive control,” in *Proc. 49th IEEE Conf. Decis. Control (CDC)*, Dec. 2010, pp. 1767–1772.

[26] M. Kanamori and K. Iwagami, “Finite-gain L_2 stability for position/force control of robot manipulators with constraint uncertainties,” in *Proc. Int. Conf. Methods Models Automationand Robot.*, 2015, pp. 1104–1109.

[27] I. Karafyllis, M. Kontorinaki, and M. Krstic, “Adaptive control by regulation-triggered batch least squares,” *IEEE Trans. Autom. Control*, vol. 65, no. 7, pp. 2842–2855, Jul. 2020.

[28] R. Ortega, J. G. Romero, and S. Aranovskiy, “A new least squares parameter estimator for nonlinear regression equations with relaxed excitation conditions and forgetting factor,” 2022, *arXiv:2205.00099*.

[29] C. Desoer and M. Vidyasagar, “Linear systems,” in *Feedback Systems: Input-Output Properties*. New York, NY, USA: Academic, 1975, pp. 56–135.

[30] B. O. Anderson and R. Johnstone, “Robust Lyapunov stability results and adaptive systems,” in *Proc. 20th IEEE Conf. Decis. Control Including Symp. Adapt. Processes*, Dec. 1981, pp. 510–515.

[31] A. Nagurney and D. Zhang, *Projected Dynamical Systems and Variational Inequalities With Applications*. Norwell, MA, USA: Kluwer, 1996.

[32] J. Parkum, N. Poulsen, and J. Holst, “Selective forgetting in adaptive procedures,” in *Proc. IFAC World Congr.*, Tallinn, Estonia, 1990, pp. 137–142.

[33] J. Love, *Least Squares Identification. In: Process Automation Handbook: A Guide to Theory and Practice*. London, U.K.: Springer, 2007.

[34] K. Åström and B. Wittenmark, *Adaptive Control* (Dover Books on Electrical Engineering), 2nd ed. Mineola, NY, USA: Dover, 2008.

[35] L. Ljung and T. Söderström, *Theory and Practice OF Recursive Identification*. Cambridge, MA, USA: MIT Press, 1983.

[36] D. P. Bertsekas, *Constrained Optimization and Lagrange Multiplier Methods*. New York, NY, USA: Academic, 1996.

Michael Schwegel received the B.S. degree in process engineering and the M.S. degree in mechanical engineering from TU Wien, Vienna, Austria, in 2013 and 2016, respectively.

He is currently employed as a Research Assistant with the Automation and Control Institute (ACIN), TU Wien. His research interests include mechatronic systems, robotics, learning systems, and nonlinear control algorithms.

Tobias Glück (Member, IEEE) received the Dipl.-Ing. degree in technical cybernetics from the University of Stuttgart, Stuttgart, Germany, in 2007, and the Ph.D. degree from TU Wien, Vienna, Austria, in 2013.

He is currently with the AIT Austrian Institute of Technology GmbH, Vienna. His work focuses on thinking in systems and the holistic view on automation components and production processes. He develops and implements methods, algorithms, and technologies to optimize and control these complex dynamical systems.

Vitaly Shaferman received the B.Sc. *(summa cum laude)*, M.A., and Ph.D. degrees from the Faculty of Aerospace Engineering, Technion—Israel Institute of Technology, Haifa, Israel, in 1995, 2008, and 2011, respectively. He is also a Distinguished Graduate of the U.S. Air Force Test Pilot School, Edwards AFB, CA, USA.

From 2014 to 2016, he was a Post-Doctoral Fellow with the Automation and Control Institute (ACIN), TU-Wien, Vienna University of Technology, Vienna, Austria. He is currently an Associate Professor at the Faculty of Aerospace Engineering, Technion–Israel Institute of Technology. His research focuses on guidance, navigation, and control (GNC) of autonomous aerial and space vehicles.

Luca Zaccarian (Fellow, IEEE) received the Ph.D. degree from the University of Roma Tor Vergata, Rome, Italy, in 2000.

He has been an Assistant Professor in control engineering with the University of Roma Tor Vergata, from 2000 to 2006, and then an Associate Professor. Since 2012, he has been the Directeur de Recherche with LAAS-CNRS, Toulouse, France, and since 2013, he holds a part-time professor position with the University of Trento, Trento, Italy. His main research interests include analysis and design of nonlinear and hybrid control systems, modeling, and control of mechatronic systems.

Dr. Zaccarian is a fellow of the IEEE Class of 2016. He was a recipient of the 2001 O. Hugo Schuck Best Paper Award given by the American Automatic Control Council.

Andreas Kugi (Senior Member, IEEE) received the Dipl.-Ing. degree in electrical engineering from TU Graz, Graz, Austria, in 1992, and the Ph.D. degree in control engineering from Johannes Kepler University (JKU), Linz, Austria, in 1995.

In 2000, he got the Habilitation in the field of control theory and automatic control with JKU and he was a Full Professor for system theory and automatic control with Saarland University, Saarbrücken, Germany, from 2002 to 2007. Since June 2007, he has been a Full Professor for complex dynamical systems and the Head of the Automation and Control Institute, TU Wien, Vienna, Austria, and since 2017, he has been the Head of the Center for Vision, Automation & Control, Automation & Control, AIT Austrian Institute of Technology GmbH, Vienna, Austria. His main research interests include the modeling, nonlinear control and optimization of complex dynamical systems, the mechatronic system design, as well as robotics and process automation.

Dr. Kugi is a full member of the Austrian Academy of Sciences and a member of the German National Academy of Science and Engineering (acatech).